Control and Detection of Singlet-Triplet Mixing in a Random Nuclear Field

F. H. L. Koppens *et al.*

Science **309**, 1346 (2005);
DOI: 10.1126/science.1113719

gitudinal moment changes. For UGe_2 the superconducting coupling strength and transition temperature increase as the magnetic transition is approached by tuning the pressure (*20*). The magnetic transition is, however, first order (*21*), and UGe_2 has not yet been studied under the conditions necessary to drive it to a QCEP. The apparent relationship of high field superconductivity to a field-induced quantum critical point in URhGe established here, however, reinforces the general notion that new strongly correlated electron ground states emerge close to quantum critical transitions between apparently simpler magnetic phases. An interesting possibility is that the low field superconductivity in URhGe might also be related to the same quantum critical point that we now outline. Superconductivity occurs when the upper critical field for the superconducting state, H_{c2}, exceeds the total magnetic field acting on the electrons. For URhGe, as the applied field is reduced from H_R moving the material away from the QCEP, H_{c2} is expected to fall rapidly. Superconductivity would disappear when H_{c2} falls below the applied field (for simplicity, the small internal field in the sample due to its magnetization, $\mu_0 M \approx 0.1$ T, can be ignored). However, if H_{c2} is still finite at low fields, the condition for superconductivity (with a much weaker coupling strength) would once again be fulfilled when the applied field is reduced to zero.

References and Notes

1. N. D. Mathur *et al.*, *Nature* **394**, 39 (1998).
2. S. S. Saxena *et al.*, *Nature* **406**, 587 (2000).
3. D. Aoki *et al.*, *Nature* **413**, 613 (2001).
4. F. Hardy, A. D. Huxley, *Phys. Rev. Lett.* **94**, 247006 (2005).
5. Evidence for a metamagnetic transition, although ascribed to fields applied parallel to a different crystal axis, can be found in an unpublished report (*22*).
6. H. W. Meul *et al.*, *Phys. Rev. Lett.* **53**, 497 (1984).
7. T. Konoike *et al.*, *Phys. Rev. B* **70**, 94514 (2004).
8. S. Uji *et al.*, *Nature* **410**, 908 (2001).
9. S. Uji *et al.*, *Phys. Rev. B* **71**, 104525 (2005).
10. V. Jaccarino, M. Peter, *Phys. Rev. Lett.* **9**, 290 (1962).
11. D. Fay, J. Appel, *Phys. Rev. B* **22**, 3173 (1980).
12. R. Roussev, A. J. Millis, *Phys. Rev. B* **63**, 140504 (2001).
13. T. R. Kirkpatrick *et al.*, *Phys. Rev. Lett.* **87**, 127003 (2001).
14. E. M. Lifshitz, L. P. Pitaevskii, *Statistical Physics Part 2, Landau and Lifshitz Course of Theoretical Physics* (Butterworth-Heinemann, Oxford, 1991), vol. 9.
15. V. P. Mineev, *Phys. Rev. B* **66**, 134504 (2002).
16. J. Custers *et al.*, *Nature* **424**, 524 (2003).
17. S. A. Grigera *et al.*, *Science* **306**, 1154 (2004).
18. N. Harrison, M. Jaime, J. A. Mydosh, *Phys. Rev. Lett.* **90**, 096402 (2003).
19. G. G. Lonzarich, in *Electron: A Centenary Volume*, M. Springford, Ed. (Cambridge Univ. Press, Cambridge, 1997), ch. 6.
20. I. Sheikin *et al.*, *Phys Rev. B* **64**, 220503(R) (2001).
21. C. Pfleiderer, A. D. Huxley, *Phys. Rev. Lett.* **89**, 147005 (2002).
22. K. Prokes, unpublished data.
23. A description of experimental methods can be found in supplementary material on *Science* Online.

24. We thank F. Hardy for contributions to the early stages of the present study. We also acknowledge useful discussions with A. Green, A. Mackenzie, V. Mineev, and M. Zhitomirsky.

Supporting Online Material

www.sciencemag.org/cgi/content/full/309/5739/1343/DC1

Materials and Methods

31 May 2005; accepted 3 August 2005

10.1126/science.1115498

Control and Detection of Singlet-Triplet Mixing in a Random Nuclear Field

F. H. L. Koppens,[1]* J. A. Folk,[1]* J. M. Elzerman,[1] R. Hanson,[1] L. H. Willems van Beveren,[1] I. T. Vink,[1] H. P. Tranitz,[2] W. Wegscheider,[2] L. P. Kouwenhoven,[1] L. M. K. Vandersypen[1]†

We observed mixing between two-electron singlet and triplet states in a double quantum dot, caused by interactions with nuclear spins in the host semiconductor. This mixing was suppressed when we applied a small magnetic field or increased the interdot tunnel coupling and thereby the singlet-triplet splitting. Electron transport involving transitions between triplets and singlets in turn polarized the nuclei, resulting in marked bistabilities. We extract from the fluctuating nuclear field a limitation on the time-averaged spin coherence time T_2^* of 25 nanoseconds. Control of the electron-nuclear interaction will therefore be crucial for the coherent manipulation of individual electron spins.

A single electron confined in a GaAs quantum dot is often referred to as artificial hydrogen. One important difference between natural and artificial hydrogen, however, is that in the first, the hyperfine interaction couples the electron to a single nucleus, whereas in artificial hydrogen, the electron is coupled to about one million Ga and As nuclei. This creates a subtle interplay between electron spin eigenstates affected by the ensemble of nuclear spins (the Overhauser shift), nuclear spin states affected by time-averaged electron polarization (the Knight shift), and the flip-flop mechanism that trades electron and nuclear spins (*1*, *2*).

The electron-nuclear interaction has important consequences for quantum information processing with confined electron spins (*3*). Any randomness in the Overhauser shift introduces errors in a qubit state, if no correcting measures are taken (*4*–*6*). Even worse, multiple qubit states, like the entangled states of two coupled electron spins, are redefined by different Overhauser fields. Characterization and control of this mechanism will be critical both for identifying the problems and finding potential solutions.

We studied the implications of the hyperfine interaction on entangled spin states in two coupled quantum dots—an artificial hydrogen molecule—in which the molecular states could be controlled electrically. A random polarization of nuclear spins creates an inhomogeneous effective field that couples molecular singlet and triplet states and leads to new eigenstates that are admixtures of these two. We used transport measurements to determine the degree of mixing over a wide range of tunnel coupling and observed a subtle dependence of this mixing on magnetic field. We found that we could controllably suppress the mixing by increasing the singlet-triplet splitting. This ability is crucial for reliable two-qubit operations such as the SWAP gate, which interchanges the spin states of the two dots (*3*).

Furthermore, we found that electron transport itself acts back on the nuclear spins through the hyperfine interaction, and time-domain measurements revealed complex, often bistable, behavior of the nuclear polarization. Understanding the current-induced nuclear polarization is an important step toward electrical control of nuclear spins. Such control will be critical for electrical generation and detection of entangled nuclear spin states (*7*) and for transfer of quantum information between electron and nuclear spin systems (*8*, *9*). It may also be possible to control the nuclear field fluctuations themselves in order to achieve longer electron spin coherence times (*10*–*12*).

We investigated the coupled electron-nuclear system using electrical transport measurements through two dots in series (*13*), in a regime where the Pauli exclusion principle blocks current flow (*14*, *15*). The dots were defined with electrostatic gates on a GaAs/AlGaAs heterostructure (Fig. 1E) (*16*). The gate voltages were tuned such that one electron always resides in the right dot, and a second electron could tunnel from the left reservoir, through the left and right dots, to the right reservoir (Fig. 1D). This current-carrying cycle can be described with the occupations (m, n) of the left and right dots: $(0,1) \rightarrow (1,1) \rightarrow$

[1]Kavli Institute of Nanoscience, Delft University of Technology, Post Office Box 5046, 2600 GA Delft, Netherlands. [2]Institut für Angewandte und Experimentelle Physik, Universität Regensburg, Regensburg, Germany.

*These authors contributed equally to this work.

†To whom correspondence should be addressed. E-mail: lieven@qt.tn.tudelft.nl

(0,2) → (0,1). When an electron enters from the left dot, the two-electron system forms either a molecular singlet, S(1,1), or a molecular triplet, T(1,1). From S(1,1), the electron in the left dot can move to the right dot to form S(0,2). From T(1,1), however, the transition to (0,2) is forbidden by spin conservation [T(0,2) is much higher in energy than S(0,2)]. Thus, as soon as T(1,1) is occupied, further current flow is blocked (we refer to this effect as Pauli blockade).

A characteristic measurement of this blockade is shown in Fig. 1A. The suppression of current (<80 fA) in the region defined by dashed lines is a signature of Pauli blockade (*14*, *15*) (fig. S1 and supporting text). Fig. 1B shows a similar measurement, but with a much weaker interdot tunnel coupling *t*. Strikingly, a large leakage current appears in the Pauli blockaded region, even though the barrier between the two dots is more opaque. Furthermore, this leakage current was substantially reduced by an external magnetic field of only 100 mT (Fig. 1C). Such a strong field dependence is unexpected at first glance, because the in-plane magnetic field, B_{ext}, couples primarily to spin but the Zeeman energies (E_Z) involved are very small ($E_Z \sim 2.5$ μeV at $B_{ext} = 100$ mT, as compared with a thermal energy of ~15 μeV at 150 mK, for example).

Leakage in the Pauli blockade regime occurs when singlet and triplet states are coupled. The T(1,1) that would block current can then transition to the S(1,1) state and the blockade is lifted (Fig. 1D). As we will show, coupling of singlets and triplets (Fig. 1, B and C) in our measurements is caused by the hyperfine interaction between the electron spins and the Ga and As nuclear spins [other leakage mechanisms can be ruled out (supporting text)].

The hyperfine interaction between an electron with spin $\vec{S}$ and a nucleus with spin $\vec{I}$ has the form $(A\vec{I} \cdot \vec{S})$, where *A* characterizes the coupling strength. An electron coupled to an ensemble of *n* nuclear spins experiences an effective magnetic field $\vec{B_N} \sim \frac{1}{(g\mu_B)} \sum_i^n A_i \vec{I}_i$, with *g* the electron *g* factor and μ_B the Bohr magneton (*1*). For fully polarized nuclear spins in GaAs, $B_N \sim 5$ T (*17*). For unpolarized nuclear spins, statistical fluctuations give rise to an effective field pointing in a random direction with an average magnitude of $5\ \mathrm{T}/\sqrt{n}$ (*4*, *5*, *18*). Quantum dots like those measured here contain $n \sim 10^6$ nuclei, so $\|\vec{B_N}\| \sim 5$ mT.

Nuclei in two different dots give rise to effective nuclear fields, $\vec{B_{N1}}$ and $\vec{B_{N2}}$, that are uncorrelated. Although the difference in field $\Delta\vec{B_N} = \vec{B_{N1}} - \vec{B_{N2}}$ is small, corresponding to an energy $E_N \equiv g\mu_B\|\Delta\vec{B_N}\| \sim 0.1$ μeV, it nevertheless plays a critical role in Pauli blockade. The (1,1) triplet state that blocks current flow consists of one electron on each of the two dots. When these two electrons are subject to different fields, the triplet is mixed with the singlet and Pauli blockade is lifted. For instance, an inhomogeneous field along $\hat{z}$ causes the triplet $|T_0\rangle = \frac{1}{\sqrt{2}}(|\uparrow\downarrow\rangle + |\downarrow\uparrow\rangle)$ to evolve into the singlet $\frac{1}{\sqrt{2}}(|\uparrow\downarrow\rangle - |\downarrow\uparrow\rangle)$. Similarly, the evolution of the other two triplet states, $|T_+\rangle = |\uparrow\uparrow\rangle$ and $|T_-\rangle = |\downarrow\downarrow\rangle$, into the singlet is caused by $\hat{x}$ and $\hat{y}$ components of $\Delta\vec{B_N}$.

The degree of mixing by the inhomogeneous field depends on the singlet-triplet energy splitting, E_{ST}. Singlet and triplet states that are close together in energy ($E_{ST} \ll E_N$) are strongly mixed, whereas the perturbation caused by the nuclei on states far apart in energy ($E_{ST} \gg E_N$) is small.

The singlet-triplet splitting depends on the interdot tunnel coupling *t* and on the detuning of left and right dot potentials Δ_{LR}. Δ_{LR} and *t* were controlled experimentally with gate voltages (Fig. 1E). Gate voltage V_t controlled the interdot tunnel coupling. V_L and V_R set the detuning, and thereby determined whether transport was inelastic (detuned levels), resonant (aligned levels), or blocked by Coulomb blockade (Fig. 1F). The coupling of the dots to the leads was held constant with V_{lead}.

The effect of the two tunable parameters *t* and Δ_{LR} on the singlet and triplet energies is illustrated in Fig. 2, A and B. For weak tunnel coupling ($t \sim 0$), and in the absence of a hyperfine interaction ($E_N \sim 0$), the (1,1) singlet and (1,1) triplet states are nearly degenerate (Fig. 2A). A finite interdot tunnel coupling *t* leads to an anticrossing of S(1,1) and S(0,2). The level repulsion results in an increased singlet-triplet splitting that is strongly dependent on detuning (Fig. 2B). At the resonant condition ($\Delta_{LR} = 0$, aligned levels), the

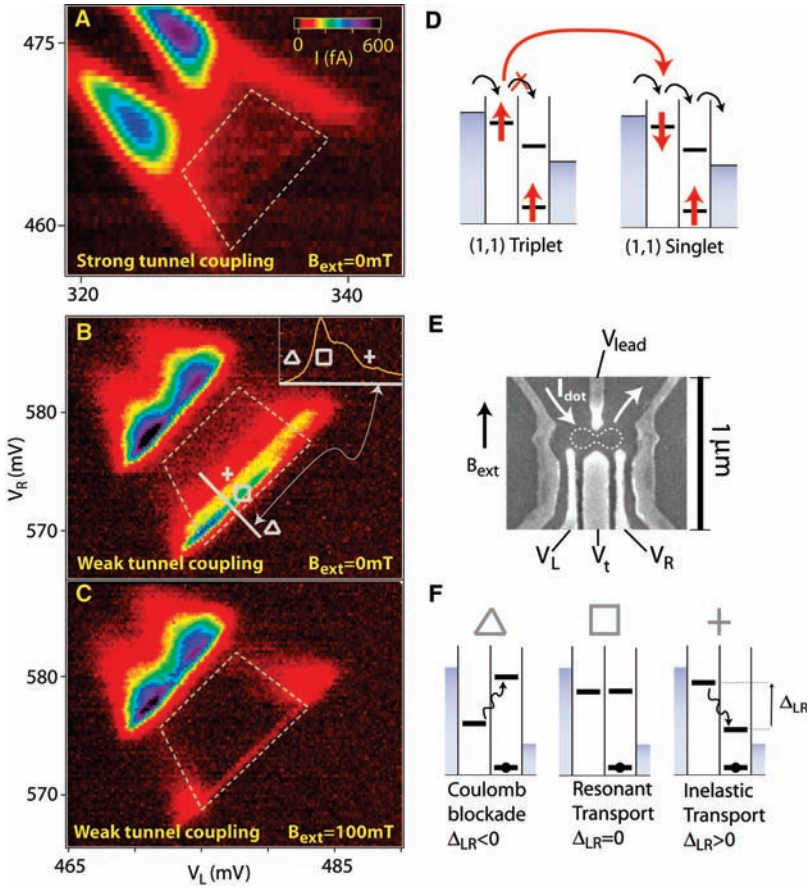

Fig. 1. Pauli blockade and leakage current. (**A**) Color-scale plot of the current through two coupled dots as a function of the left and right dot potentials (voltage bias, 800 μeV; $V_t = -108$ mV). The experimental signature of Pauli blockade is low current (<80 fA) in the area denoted by dashed gray lines. (**B**) Analogous data for smaller interdot tunnel coupling ($V_t = -181$ mV), with the same color scale as in (A). A marked increase of leakage current is seen in the lower part of the Pauli blockaded area (the green and yellow band). Inset: One-dimensional trace along the solid gray line, with Coulomb blockaded, resonant, and inelastic transport regimes marked as defined in (F). (**C**) Analogous data for the same tunnel coupling as in (B), but for $B_{ext} = 100$ mT. The leakage current from (B) is strongly suppressed. (**D**) Two level diagrams that illustrate Pauli blockade in coupled quantum dots. When the (1,1) triplet evolves to a (1,1) singlet (red arrow), Pauli blockade is lifted. (**E**) Scanning electron micrograph showing the device geometry. White arrows indicate current flow through the two coupled dots (dotted line). (**F**) Level diagrams illustrating three transport regimes. △: Coulomb blockade; transport would require absorption of energy. □: Resonant transport; the dot levels are aligned. +: Inelastic transport; energy must be transferred to the environment, for instance, by emitting a phonon.

two new singlet eigenstates are equidistant from the triplet state, both with $E_{ST} = \sqrt{2}t$. For finite detuning (finite but still smaller than the single dot S-T splitting), one singlet state comes closer to the triplet state ($E_{ST} \sim t^2/\Delta_{LR}$), whereas the other moves away. In Fig. 2, A and B, singlet and triplet states are pure eigenstates (not mixed), and therefore Pauli blockade would be complete.

The additional effect of the inhomogeneous nuclear field is shown in Fig. 2, C and D. For small t ($\sqrt{2}t$, $t^2/\Delta_{LR} < E_N$), the (1,1) singlet and (1,1) triplet are close together in energy and therefore strongly mixed (purple lines) over the entire range of detuning. For t such that $t^2/\Delta_{LR} < E_N < \sqrt{2}t$, triplet and singlet states mix strongly only for finite detuning. This is because E_{ST} is larger than E_N for aligned levels but smaller than E_N at finite detuning. For still larger t ($\sqrt{2}t$, $t^2/\Delta_{LR} > E_N$, not shown in Fig. 2), mixing is weak over the entire range of detuning. In the cases where mixing between S and T is strong, as in Fig. 2, C and D (for large detuning), Pauli blockade is lifted and a leakage current results.

The competition between E_{ST} and E_N can be seen experimentally by comparing one-dimensional traces of leakage current as a function of detuning over a wide range of t (Fig. 3A). Resonant current appears as a peak at $\Delta_{LR} = 0$ and inelastic leakage as the shoulder at $\Delta_{LR} > 0$ (*19*). When the interdot tunnel coupling was small, both resonant and inelastic transport were allowed because of singlet-triplet mixing, and both rose as the middle barrier became more transparent. As the tunnel coupling was raised further, a point was reached where E_{ST} became larger than the nuclear field and Pauli blockade suppressed the current (Fig. 1A). The maximum resonant current occurred at a smaller value of t compared to the maximum inelastic current (Fig. 3A,

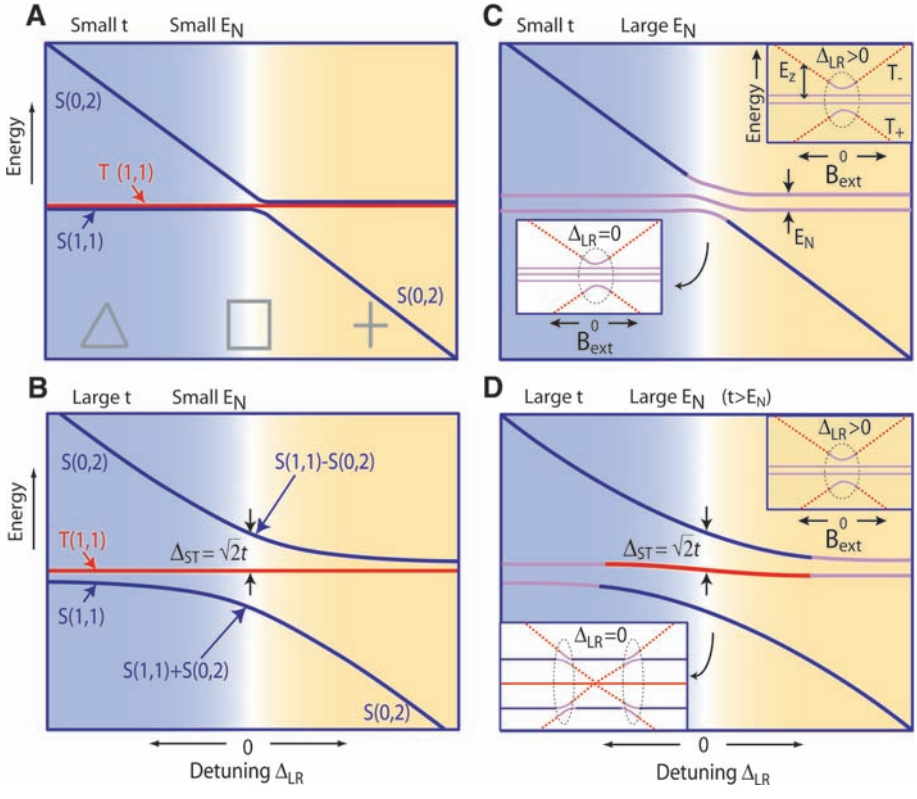

Fig. 2. Two-electron level diagrams showing energy as a function of detuning Δ_{LR}. Detuning is defined so that the energy of T(1,1) remains constant as Δ_{LR} varies (fig. S1B and supporting text). T(0,2) is not shown as it occurs far above the energies shown here. The panels on the left illustrate the effect of t; the panels on the right include the additional effect of an inhomogeneous magnetic field. Pure singlet and triplet states are drawn in blue and red, respectively; strong admixtures are in purple. The blue (△), white (□), and yellow (+) background corresponds to the Coulomb blockade, resonant, and inelastic transport regimes, respectively. **(A)** For small tunnel coupling, T(1,1) and S(1,1) are nearly degenerate. **(B)** For finite t, level repulsion between the singlet states results in a larger singlet-triplet splitting than shown in (A), which depends on detuning. The tunnel coupling does not mix singlet and triplet states. For large Δ_{LR} (that are still smaller than the single dot S-T splitting), $E_{ST} \sim t^2/\Delta_{LR}$. **(C** and **D)** An inhomogeneous field mixes triplet and singlet states that are close in energy (purple lines). For clarity, only one triplet state is shown in the main panels. (C) For small t, T(1,1) and S(1,1) mix strongly over the full range of detuning. (D) For large t, T(1,1) mixes strongly with the singlet only for large detuning. The insets to (C) and (D) show the effect of an external magnetic field on the two-electron energy levels. All three triplets are shown in the insets; the triplets $|T_+\rangle$ and $|T_-\rangle$ split off from $|T_0\rangle$ because of B_{ext}. The leakage current is highest in the regions indicated by black dotted ellipses.

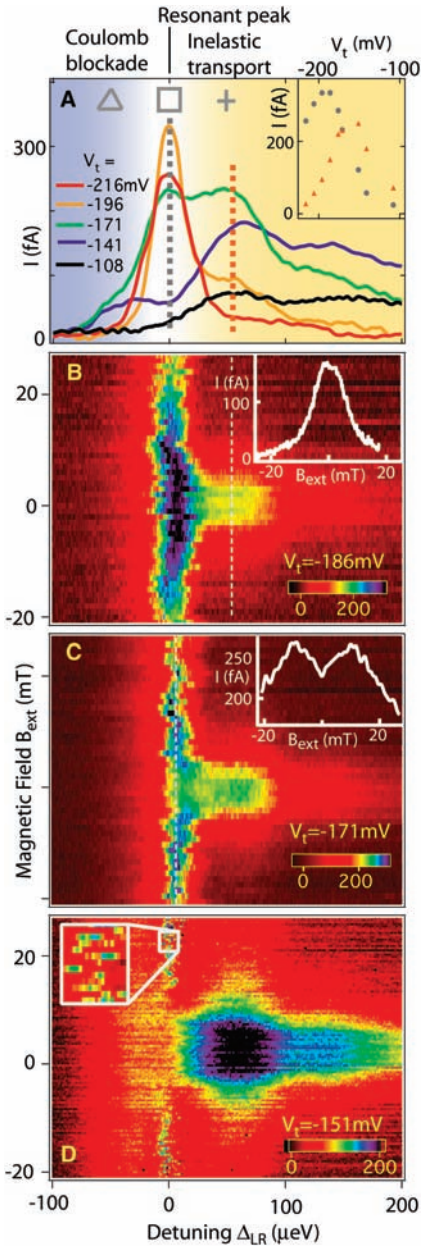

Fig. 3. The measured leakage current results from a competition between E_N, E_{ST}, and E_Z. **(A)** One-dimensional traces of the leakage current as a function of detuning at $B_{ext} = 0$, for a wide range of tunnel couplings (analogous to the inset of Fig. 1B). Coulomb blockade, resonant transport, and inelastic transport are indicated as in Fig. 2. Inset: Leakage current along the dotted gray and orange lines is shown as a function of V_t. Resonant and inelastic leakage (gray and orange markers) reach a maximum at different tunnel couplings ($V_t = -190$ mV and -150 mV, respectively). **(B)** For small tunnel coupling ($<E_N$), both the resonant and inelastic leakage currents drop monotonically with B_{ext}. Inset: Magnetic field dependence of the inelastic current along the dotted line ($\Delta_{LR} = 40$ μeV). **(C)** For larger t ($>E_N$), the resonant leakage current is maximum at $B_{ext} = 10$ mT. Inset: Field dependence of the resonant peak height (dotted line). **(D)** For still larger t, the resonant current is strongly reduced at low field (main panel), then becomes unstable for higher field (inset).

inset). This is consistent with E_{ST} being much smaller for finite detuning than for aligned levels ($t^2/\Delta_{LR} \ll \sqrt{2}t$) (Fig. 2, B and D).

The experimental knob provided by electrostatic gates is very coarse on the energy scales relevant to the hyperfine interaction. However, the external magnetic field can easily be controlled with a precision of 0.1 mT, corresponding to a Zeeman splitting (2 neV) that is 50 times smaller than E_N. For this reason, monitoring the field dependence allowed a more detailed examination of the competing energy scales E_{ST}, E_Z, and E_N.

The competition between E_Z and E_N is clear for small interdot tunnel coupling (Fig. 3B). Leakage current was suppressed monotonically with the magnetic field, on a scale of ~5 mT and ~10 mT for inelastic and resonant transport, respectively. The qualitative features of this field dependence can be understood from the insets to Fig. 2C. At zero field, all states are mixed strongly by the inhomogeneous nuclear field, but when E_Z exceeds E_N, the mixing between the singlet and two of the triplet states ($|T_+\rangle$ and $|T_-\rangle$) is suppressed. An electron loaded into either of these blocks further current flow, explaining the disappearance of leakage at high field in the measurement.

The magnitude of the fluctuating Overhauser field can be extracted from the inelastic peak shape in the limit of small t (Fig. 3B, inset). We fit the data to a model that describes the transport cycle with the density matrix approach (*20*) (supporting text). From this fit, we found the magnitude of the inhomogeneous field $\sqrt{\langle \Delta B_N^2 \rangle} = 1.73 \pm 0.02$ mT ($E_N = 0.04$ μeV), largely independent of Δ_{LR} over the parameter range studied (*21*). The value for the effective nuclear field fluctuations in a single dot was obtained from the relation $\langle B_N^2 \rangle = \frac{1}{2}\langle \Delta B_N^2 \rangle$, giving $\sqrt{\langle B_N^2 \rangle} = 1.22$ mT. This is consistent with the strength of the hyperfine interaction in GaAs and the number of nuclei that are expected in each dot (*4*, *22*).

The three-way interplay between E_{ST}, E_Z, and E_N is most clearly visible in the resonant current. At an intermediate value of tunnel coupling, $t \gtrsim E_N$ (Fig. 3C), the resonant peak was split in magnetic field, with maxima at ±10 mT (Fig. 3C, inset). The lower inset to Fig. 2D illustrates this behavior. At $B_{ext} = 0$, the resonant current in Fig. 3C was suppressed compared to the current in Fig. 3B, because E_{ST} was greater than E_N at that point. Increasing B_{ext} enhanced the mixing as the $|T_+\rangle$ and $|T_-\rangle$ states approached the singlet states. The maximum leakage occurred when the states crossed, at E_{ST} (= $\sqrt{2}t$) = E_Z. Here, E_Z was 0.25 ± 0.03 μeV at the current maximum, from which we extract $t = 0.18 \pm 0.02$ μeV for this setting of V_t. At still larger B_{ext}, $|T_+\rangle$ and $|T_-\rangle$ moved away from the singlet states again, and the leakage current was suppressed.

The system entered into a new regime for still higher tunnel coupling (Figs. 3D and 4), where it became clear that the electron-nuclear system is dynamic. The zero field resonant leakage was further suppressed, and above 10 mT, prominent current spikes appeared (Fig. 3D, inset). The spikes are markedly visible in a three-dimensional surface plot of leakage over a broader range of field (Fig. 4A). For fixed experimental parameters, the current still fluctuated in time (Fig. 4B).

We found that time-dependent behavior was a consistent feature of resonant transport for (E_{ST}, E_Z) ≫ E_N. For some device settings, the time dependence was fast (for example, the fluctuations in Fig. 4, A and B), but for others, the leakage changed much more slowly (Fig. 4C). Starting from an equilibrium situation (bias voltage switched off for 5 min), the current was initially very small after the bias was turned on. It built up and then saturated after a time that ranged from less than a second to several minutes. This time scale depended on Δ_{LR}, t, and B_{ext}. When no voltage bias was applied, the system returned to equilibrium after ~80 s at 200 mT. Similar long time scales of the nuclear spin-lattice relaxation times have been reported before in GaAs systems (*23*) and quantum dots (*24*). We thus associate the slow time dependence observed in our system with current-induced dynamic nuclear polarization and relaxation.

Evidence that the fast fluctuations too are related to current-induced nuclear polarization (and cannot be explained by fluctuating background charges alone) is found in their dependence on sweep direction and sweep rate (*23*, *25*). When the magnetic field was swept while fixed Δ_{LR} was maintained, the current showed fluctuations at low field but suddenly became stable at high field (Fig. 4D). The crossover from unstable to stable behavior occurred at a field that was hysteretic in sweep direction (Fig. 4D), and this hysteresis became more pronounced at higher sweep rates (faster than ~1 mT/s). The connection between the fluctuations and nuclear polarization is also evident from time traces, in which instability developed only after the nuclear polarization was allowed to build for some time (fig. S3).

Unlike the regular oscillations that have been observed in other GaAs structures (*1*, *26*),

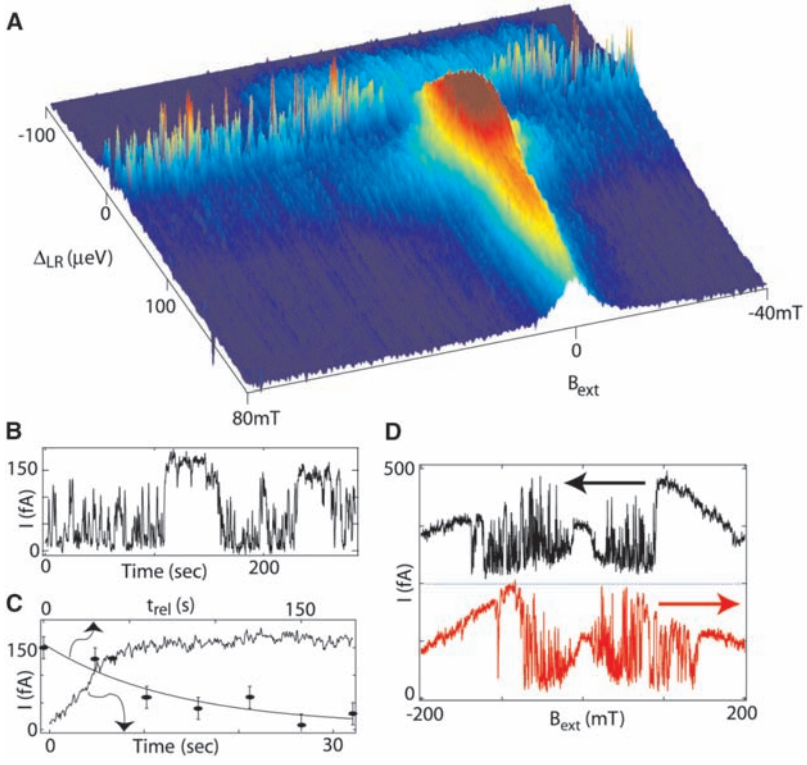

Fig. 4. Time dependence of the leakage current reveals the dynamics of the electron-nuclear system. This time dependence occurs in the regime corresponding to Fig. 2D. (**A**) Surface plot of electrical transport for $V_t = -151$ mV. Instability on the resonant peak is visible as sharp current spikes. The sweep direction is from positive to negative Δ_{LR}, for fields stepped from negative to positive B_{ext}. (**B**) Explicit time dependence of the resonant current exhibits bistability ($V_t = -141$ mV, $B_{ext} = 100$ mT). (**C**) Lower axis: Dynamic nuclear polarization due to electron transport through the device ($V_t = -141$ mV, $\Delta_{LR} = 0$, $B_{ext} = 200$ mT), after initialization to zero polarization by waiting for 5 min with no voltage applied. Top axis: In order to measure the nuclear spin relaxation time, we waited for the current to saturate, switched off the bias voltage for a time t_{rel}, and then remeasured the leakage current. An exponential fit gives a time constant of 80 ± 40 s (measurements of these long time scales result in large error bars, ±20 fA, because of 1/f noise). (**D**) The field dependence of the resonant current is hysteretic in the sweep direction ($V_t = -149$ mV). Each trace takes ~7 min.

the fluctuations in our measurements were random in time and, in many cases, suggested bistability with leakage current moving between two stable values. We discuss the origin of such fast bistable fluctuations in the supporting text.

The ensemble of random nuclear spins that gives rise to the mixing of two-electron states as observed in this experiment also gives rise to an uncertainty of $g\mu_B \sqrt{\langle {B_N}^2 \rangle} = 0.03$ μeV in the Zeeman splitting of one electron. When averaged over a time longer than the correlation time of the nuclear spin bath (~100 μs) (*27*), this implies an upper limit on the time-averaged spin coherence time of $T_2^* = (\frac{\hbar}{2\pi})/g\mu_B\sqrt{\langle \frac{2}{3}{B_N}^2 \rangle} = 25$ ns [as defined by Merkulov *et al.* (*4*)], comparable to the T_2^* found in recent optical spectroscopy measurements (*28*). This value is four orders of magnitude shorter than the theoretical prediction for the electron spin T_2 in the absence of nuclei, which is limited only by spin-orbit interactions (*29*–*31*).

One way to eliminate the uncertainty in Zeeman splitting that leads to effective dephasing is to maintain a well-defined nuclear spin polarization (*12*). Many of the regimes explored in this paper show leakage current that is stable when current-induced polarization is allowed to settle for some time. These may in fact be examples of specific nuclear polarizations that are maintained electrically.

References and Notes

1. F. Meier, B. P. Zakharchenya, Eds., *Optical Orientation* (North-Holland, New York, 1984).
2. D. Gammon *et al.*, *Science* **277**, 85 (1997).
3. D. Loss, D. P. DiVincenzo, *Phys. Rev. A.* **57**, 120 (1998).
4. I. A. Merkulov, A. L. Efros, J. Rosen, *Phys. Rev. B* **65**, 205309 (2002).
5. P.-F. Braun *et al.*, *Phys. Rev. Lett.* **94**, 116601 (2005).
6. A. S. Bracker *et al.*, *Phys. Rev. Lett.* **94**, 047402 (2005).
7. M. Eto, T. Ashiwa, M. Murata, *J. Phys. Soc. Jpn.* **73**, 307 (2004).
8. B. E. Kane, *Nature* **393**, 133 (1998).
9. J. M. Taylor, A. Imamoglu, M. D. Lukin, *Phys. Rev. Lett.* **91**, 246802 (2003).
10. J. Schliemann, A. Khaetskii, D. Loss, *J. Phys. Condens. Matter* **15**, R1809 (2003).
11. A. V. Khaetskii, D. Loss, L. Glazman, *Phys. Rev. Lett.* **88**, 186802 (2002).
12. W. A. Coish, D. Loss, *Phys. Rev. B* **70**, 195340 (2004).
13. W. G. van der Wiel *et al.*, *Rev. Mod. Phys.* **75**, 1 (2003).
14. K. Ono, D. G. Austing, Y. Tokura, S. Tarucha, *Science* **297**, 1313 (2002).
15. A. C. Johnson, J. R. Petta, C. M. Marcus, M. P. Hanson, A. C. Gossard, *cond-mat*/0410679 (2004).
16. The electrostatic gates are on the surface of a GaAs/AlGaAs heterostructure. The two-dimensional electron gas is 90 nm below the surface, with density 1.33×10^{11} cm^{-2} and mobility 9.71×10^5 cm^2/Vs. Measurements were performed in a dilution refrigerator at 150 mK, with a magnetic field in the plane of the heterostructure.
17. D. Paget, G. Lampel, B. Sapoval, V. I. Safarov, *Phys. Rev. B* **15**, 5780 (1977).
18. D. Gammon *et al.*, *Phys. Rev. Lett.* **86**, 5176 (2001).
19. T. Fujisawa *et al.*, *Science* **282**, 932 (1998).
20. O. N. Jouravlev, Y. Nazarov, personal communication.
21. The difference between the field dependence of the resonant and inelastic currents can be explained by the coupling with the leads. The S(0,2) state is lifetime-broadened because of coupling with the right lead (~0.3 μeV), giving a weaker field dependence for the resonant current. The field dependence of the inelastic leakage is not affected by the lead coupling, because under the high-bias conditions of this experiment, there were no available states in the left lead that could broaden S(1,1).
22. A. C. Johnson *et al.*, *Nature* **435**, 925 (2005).
23. M. Dobers, K. v. Klitzing, J. Schneider, G. Weimann, K. Ploog, *Phys. Rev. Lett.* **61**, 1650 (1988).
24. A. K. Hüttel *et al.*, *Phys. Rev. B* **69**, 073302 (2004).
25. The leakage current is sensitive to magnetic fields of only a few mT, corresponding to 0.1% nuclear polarization. Given that the dot has ~10^6 nuclei, changes in the nuclear polarization of 0.1% can be caused by 1000 electron-nuclear flip-flop processes. For typical currents (~100 fA), 1000 electrons move through the dot in 1 ms, so in principle current fluctuations as fast as 1 kHz are possible.
26. K. Ono, S. Tarucha, *Phys. Rev. Lett.* **92**, 256803 (2004).
27. R. de Sousa, S. Das Sarma, *Phys. Rev. B* **67**, 033301 (2003).
28. Bracker et al. (*6*) found a T_2^* of 16 ns in a GaAs quantum dot, slightly shorter than in our experiment, presumably because of a smaller dot size. Braun et al. (*5*) measured a considerably shorter time scale, 500 ps, in InAs dots, because of a notable difference in dot size, nuclear spin *I*, and the stronger hyperfine coupling constant in InAs.
29. V. N. Golovach, A. V. Khaetskii, D. Loss, *Phys. Rev. Lett.* **93**, 016601 (2004).
30. J. M. Elzerman *et al.*, *Nature* **430**, 431 (2004).
31. M. Kroutvar *et al.*, *Nature* **432**, 81 (2004).

32. We thank O. N. Jouravlev and Y. Nazarov for developing a model that helped greatly with the physical interpretation of the data; G. Burkard, W. A. Coish, V. N. Golovach, A. C. Johnson, D. Loss, and C. M. Marcus for fruitful discussions; R. Schouten, B. van den Enden, and M. van Oossanen for technical assistance; and J. Caro for supporting infrastructure. Supported by the Defense Advanced Research Projects Agency Quantum Information Science and Technology program, the Dutch Organization for Fundamental Research on Matter (FOM), the Netherlands Organization for Scientific Research (NWO), the Office of Naval Research, Exploratory Research for Advanced Technology, and the EU Research Training Network on spintronics.

Supporting Online Material

www.sciencemag.org/cgi/content/full/1113719/DC1
SOM Text
Figs. S1 to S3
References and Notes

18 April 2005; accepted 12 July 2005
Published online 21 July 2005;
10.1126/science.1113719
Include this information when citing this paper.

Gas Adsorption Sites in a Large-Pore Metal-Organic Framework

Jesse L. C. Rowsell,[1] Elinor C. Spencer,[2] Juergen Eckert,[3,4] Judith A. K. Howard,[2] Omar M. Yaghi[1]*

The primary adsorption sites for Ar and N_2 within metal-organic framework-5, a cubic structure composed of $Zn_4O(CO_2)_6$ units and phenylene links defining large pores 12 and 15 angstroms in diameter, have been identified by single-crystal x-ray diffraction. Refinement of data collected between 293 and 30 kelvin revealed a total of eight symmetry-independent adsorption sites. Five of these are sites on the zinc oxide unit and the organic link; the remaining three sites form a second layer in the pores. The structural integrity and high symmetry of the framework are retained throughout, with negligible changes resulting from gas adsorption.

Metal-organic frameworks (MOFs) have recently emerged as an important class of porous materials for their amenability to design and the flexibility with which their pores can be functionalized (*1*–*3*). In particular, their extraordinary low density (1.00 to 0.20 g/cm^3) and high surface area (500 to 4500 m^2/g) make them ideal candidates for the storage and separation of gases (N_2, Ar, CO_2, CH_4, and H_2) (*4*–*12*). In this context, identifying the gas adsorption sites in MOFs is critically important to our ability to fine-tune those sites, sterically and electronically, in order to achieve the maximum storage capacity and selectivity.

Precise determination of adsorption sites in large-pore materials remains an ongoing challenge, because the characterization techniques that are commonly applied to this problem, such as inelastic neutron scattering (INS) and diffuse reflectance infrared spectroscopy, do not provide adequate information on the structural details of the adsorption sites (*9*, *13*). The recent powder x-ray diffraction (XRD) studies of gases in MOFs (*14*, *15*) do not elucidate the nature of adsorption sites because the MOFs used have very small pores and lack the possibility of adsorbing gases on multiple sites. For large-pore structures, a more precise technique is required to determine whether adsorption sites lie on the metal oxide or the organic moieties, how many exist, and precisely where they are located in the MOF structure.

We report the detailed single-crystal XRD study of Ar and N_2 adsorbed on the internal surface of a large-pore open-framework mate-

[1]Materials Design and Discovery Group, Department of Chemistry, University of Michigan, 930 North University Avenue, Ann Arbor, MI 48109, USA. [2]Department of Chemistry, University of Durham, South Road, Durham DH1 3LE, UK. [3]Materials Research Laboratory, University of California, Santa Barbara, CA 93106, USA. [4]Los Alamos Neutron Science Center–12, Mail Stop H805, Los Alamos National Laboratory, Los Alamos, NM 87545, USA.

*To whom correspondence should be addressed. E-mail: oyaghi@umich.edu